AD-A128 988 CONVECTIVE TRANSPORT IN FLOW AROUND 180 DEG BEND(U) 1/1
UNIVERSITY OF MANCHESTER INST OF SCIENCE AND TECHNOLOGY
(ENGLAND) B E LAUNDER JAN 83 N00014-80-G-0130
UNCLASSIFIED F/G 12/1 NL

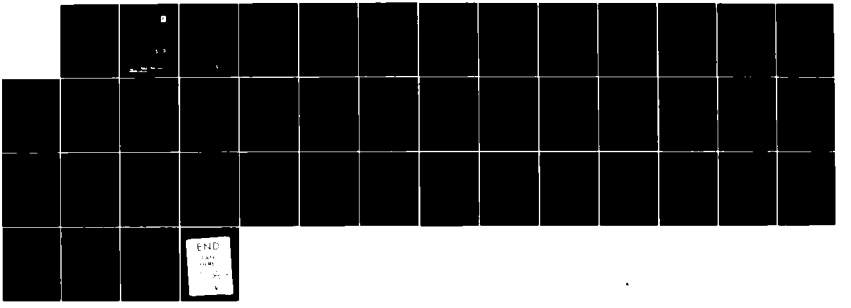

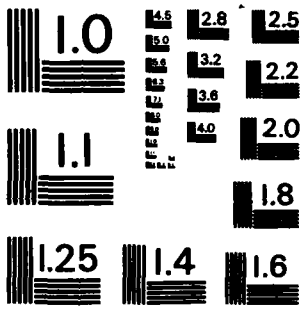

MICROCOPY RESOLUTION TEST CHART
NATIONAL BUREAU OF STANDARDS - 1963 - A

The University of Manchester Institute of Science and Technology
PO Box 88, Manchester M60 1QD. Telephone 061-236 3311. Telex 666094

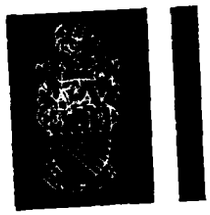

(12)

AD-A128 988

DTIC FILE COPY

DTIC
ELECTE
JUN 6 1983
S D

83 05 19 196

University of Manchester
Institute of Science & Technology

(12)

Convective Transport in Flow Around a 180° Bend

Annual Report for Period
November 1, 1981 - October 31, 1982
of Research completed under
ONR (Power Program) Research Grant
N0014-80-G-0130

Principal Investigator B.E. Launder
Research Assistant R.W. Johnson
Research Student H. Iacovides

Undertaken in collaboration with
Professor J.A.C. Humphrey, University of California, Berkeley

January 1983

Rep TFD/83/2(R)

1. INTRODUCTION

The objectives of the research program are to assess how well current numerical methods and turbulence models can combine to predict the detailed flow and heat transfer behaviour in flow around a 180° bend, a geometry of great importance in heat exchanger design and in various other cooling-passage geometries. To allow this assessment detailed flow and thermal experimental data are required - and these were not available. The total research program therefore has two roughly equal parts: obtaining the experimental data and developing and applying the 3-dimensional numerical calculation scheme.

The research has been conceived and executed as a joint effort with Professor J.A.C. Humphrey and his group at UC Berkeley. Mutual help has been provided by the two groups over the spectrum of tasks but it would be correct to say, in measurements, that the main emphasis at Berkeley has been on flow dynamics while that at UMIST has been on convective heat transfer aspects. On the computational side, the code development for the square sectioned duct has mainly proceeded at Berkeley while that for the circular sectioned tube is proceeding at UMIST (though the early development had been undertaken by Professor Humphrey in the course of his doctoral research).

The present report describes work completed at UMIST in the past year in furthering the accomplishment of the research objectives. Section 2 summarizes the computational work while progress in the experiments in presented in Section 3.

2. COMPUTATIONAL RESEARCH ON FLOW AROUND 180° BENDS

2.1 Tubes of Circular Cross-Section

2.1.1 The starting point and the path

The starting point for this work has been the three-dimensional elliptic flow code TOROID. This program was developed by Professor J.A.C. Humphrey while a Ph.D. student at Imperial College, London [1] . It is a finite-volume discretization of the steady-flow Navier-Stokes equations expressed in toroidal coordinates. It follows the structure and strategy of the TEACH family of computer programs developed at Imperial College during the 1970's through the guidance and overall coordination of Dr. A.D. Gosman.

Our aims in relation to TOROID are twofold. The first is to improve the numerics so that the code can generate, at moderate computing cost, what are sensibly accurate solutions of the equations of motion for the flow around a 180° bend. The second is to embed a high-level turbulence model (a so-called "Algebraic Stress Model" - ASM) to allow reliable predictions of flow pattern and local heat transfer rates over the turbulent flow regime for arbitrary flow entry conditions. The work completed so far has been directed at the first objective. The adaptations we wished to introduce were:

a. The incorporation of quadratic upstream differencing of convective transport (QUICK) in place of hybrid upwind differencing.

b. The improvement of boundary-condition treatments near the axis in order to remove the need for a fine grid in the centre of the flow.

c. The conversion of the code from elliptic to "semi-elliptic" in order to allow the use of fairly fine meshes.

d. The inclusion of the SIMPLER algorithm for handling the pressure-continuity connection in place of the SIMPLE scheme of the original [2].

Items a. - c. have been completed and task d. is well advanced; technical details of the work are given in sections 2.1.2 - 2.1.4.

The further steps in the code development will then be

e. Inclusion of $k\omega\epsilon$ Boussinesq viscosity model of turbulence (BVM).

f. Inclusion of wall functions developed earlier in the project.

g. Incorporation of a uniform-property ASM.

h. Inclusion of quasi-buoyant effects (associated with centrifugal pressure gradients) as a result of which the heavier eddies will be flung preferentially to the outside of the bend.

Testing and comparison with experiment will of course accompany each stage of development.

2.1.2 The Describing Equations

Figure 2.1 defines the toroidal coordinate system used to describe the flow field. In these coordinates the continuity, momentum and energy equations for a steady, uniform-density, high Reynolds, number viscous flow may, following Aris [3] , for example, be written:

Continuity

$$\frac{\partial}{\partial\phi} r_c U + \frac{\partial}{\partial r} r r_c V + \frac{\partial}{\partial\theta} r W = 0 \qquad (2.1)$$

where r_c is the local radius, $R + r\cos\phi$, and U, V and W denote velocity components in the ϕ, r and θ directions respectively.

Momentum and Energy Equations

$$\rho(C(\psi) + S_c(\psi)) = D(\psi) + S_D(\psi) + S_p(\psi) \qquad (2.2)$$

where ψ stands for any of the velocity components or the temperature T and the operators $C(\psi)$ and $D(\psi)$ stand for:

$$C(\psi) = \frac{1}{r r_c}\left[\frac{\partial}{\partial\phi}(r_c U\psi) + \frac{\partial}{\partial r}(r r_c V\psi) + \frac{\partial}{\partial\theta}(rW\psi)\right] \qquad (2.3)$$

$$D(\psi) = \frac{1}{r r_c Pr_\psi}\left[\frac{1}{r}\frac{\partial}{\partial\phi}\left(r_c\mu\frac{\partial\psi}{\partial\phi}\right) + \frac{\partial}{\partial r}\left(r r_c\mu\frac{\partial\psi}{\partial r}\right)\right] \qquad (2.4)$$

where Pr_ψ is unity for the velocity components and denotes the Prandtl number in the energy equation. The functions $S_c(\psi)$, $S_p(\psi)$ and $S_D(\psi)$ are given in Table 2.1. It will be noted that viscous terms associated with θ-direction second derivatives have been dropped, a simplification that is allowable in high Reynolds number flows.

2.1.3 Discretization

Following the strategy of the TEACH codes and other finite-volume primitive-variable procedures, the differential equations presented in Section 2.1.2 are discretized by integrating them over small contiguous control volumes which collectively cover the solution domain. To each control volume is attached a discrete value of the dependent variable. A staggered arrangement of grid nodes is adopted as indicated in figure 2.2. This choice minimizes the amount of interpolation that has to be done and improves stability.

In evaluating diffusion processes ($D(\psi)$) a linear variation of the dependent variables between adjacent nodes is assumed while the source terms ($S_p(\psi)$, $S_D(\psi)$ and $S_c(\psi)$) are mainly treated as uniform over any particular control volume. This is the standard TEACH practice.

In the original TOROID code, as provided, convective transport was handled using either an upwind or a central-difference interpolation depending on whether the modulus of the cell Peclet number was greater than or less than 2. The upwind approximation, though admirably stable, is well known to give rise to severe false diffusion if flow lines cut at appreciable angles to the cell boundaries (the error being proportional to the sine of twice the angle of incidence). A preliminary study during the first year of ONR funding (Han, Humphrey and Launder [4]) showed decisively superior results from using Leonard's [5] quadratic upwind approximation (QUICK). The principal test case in that study was the flow in a driven cavity which produced a rather similar flow pattern to that which was expected in the cross-sectional plane of the curved tube. At a cavity Reynolds number of 1000 roughly the same numerical accuracy was achieved with QUICK using one quarter as many nodes as with the upwind/central approximation. Accordingly, at the outset QUICK was incorporated into the TOROID code. In devising an approximation for the value of ψ at a point e midway between nodes i and i + 1 one interpolates on a parabola passing through these two points and through the next point on the upwind side of e. Thus

$$\text{for } U_e > 0 \quad \psi_e = \tfrac{1}{2}(\psi_i + \psi_{i+1}) - \tfrac{1}{8}(\psi_{i-1} + \psi_{i+1} - 2\psi_i)$$

ψ	$S_c(\psi)$	$S_p(\psi)$	$S_D(\psi)$
U	$\frac{VU}{r} + \{\frac{W^2 \sin\phi}{r_c}\}$	$-\frac{1}{r}\frac{\partial p}{\partial \phi}$	$\frac{1}{r_c}\frac{\partial}{\partial \phi}\{r_c\mu(\frac{\partial U}{\partial \phi} + 2V)\} + \frac{1}{rr_c}\frac{\partial}{\partial r}\{r_c\mu(\frac{\partial V}{\partial \phi} - U)\}$ $+ \mu\frac{\partial}{\partial r}\{\frac{U}{r}\} + \frac{\mu}{r^2}\frac{\partial V}{\partial \phi} + \frac{1}{r}\frac{\partial}{\partial \theta}\{\mu\frac{\partial}{\partial \phi}(\frac{W}{r_c})\}$ $- \frac{2\mu\sin\phi}{r_c^2}\{U\sin\phi - V\cos\phi - \frac{\partial W}{\partial \theta}\}$
V	$-\{\frac{\cos\phi W^2}{r^2}\}$ $-\{\frac{U^2}{r}\}$	$-\frac{\partial p}{\partial r}$	$\frac{1}{r_c}\frac{\partial}{\partial \phi}\{r_c\mu\frac{\partial}{\partial r}(\frac{U}{r})\} + \frac{1}{rr_c}\frac{\partial}{\partial r}\{rr_c\mu\frac{\partial V}{\partial r}\}$ $- \frac{2\mu}{r^2}\{\frac{\partial U}{\partial \phi} + V\} + \frac{1}{r}\frac{\partial}{\partial \theta}\{r\mu\frac{\partial}{\partial r}(\frac{W}{r_c})\}$ $+ \frac{2\mu\cos\phi}{r_c^2}\{U\sin\phi + V\cos\phi - \frac{\partial W}{\partial \theta}\}$
W	$-\{\frac{\sin\phi UW}{r_c}\}$ $+\{\frac{\cos\phi VW}{r_c}\}$	$-\frac{1}{r_c}\frac{\partial p}{\partial \theta}$	$\frac{1}{rr_c}\frac{\partial}{\partial \phi}\{\mu(\frac{\partial U}{\partial \theta} + W\sin\phi)\}$ $+ \frac{1}{rr_c}\frac{\partial}{\partial r}\{2\mu(\frac{\partial V}{\partial \theta} - W\cos\phi)\}$ $+ \frac{1}{r_c^2}\frac{\partial}{\partial \theta}\{\mu(\frac{\partial W}{\partial \theta} - 2U\sin\theta + 2V\cos\phi)\}$ $- \frac{\mu\sin\phi}{r}\frac{\partial}{\partial \phi}(\frac{W}{r_c}) + \mu\cos\phi\frac{\partial}{\partial r}(\frac{W}{r_c})$ $- \frac{\mu r\sin\phi}{r_c^2}\frac{\partial}{\partial \theta}(\frac{U}{r}) - \frac{\mu\cos\phi}{r^2}(\frac{\partial V}{\partial \theta})$
T	0	0	0

Table 2.1: Source terms for dependent variables

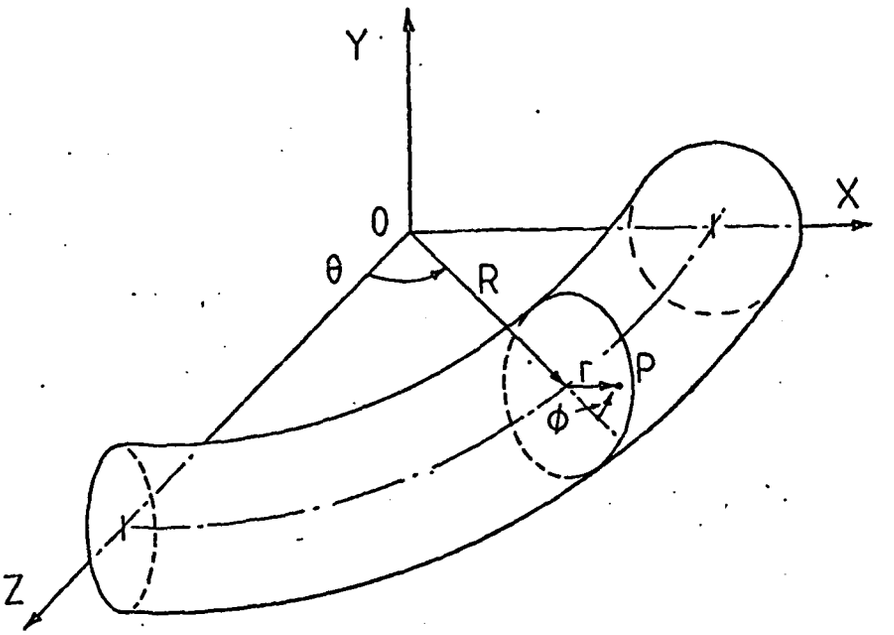

Fig. 2.1 Toroidal co-ordinate system

Uniform-θ surface

Control volume boundary for P

Control volume for V

Control volume for U

Control volume for W

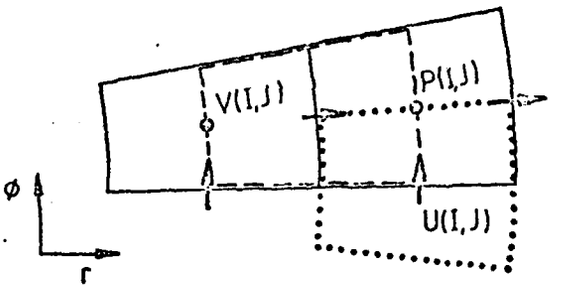

Uniform-Φ surface

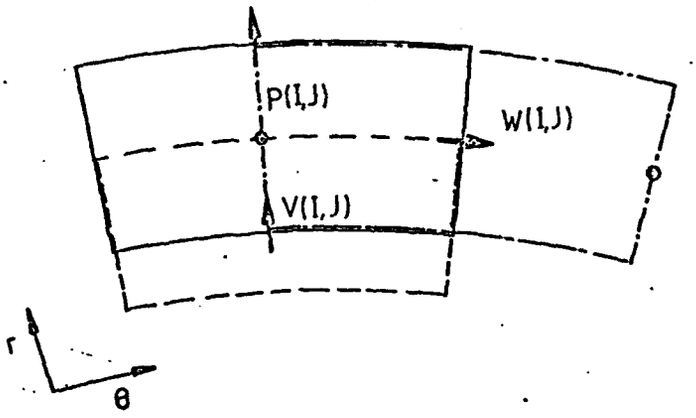

Fig. 2.2 Staggered nodes and associated control volumes

$$U_e < 0 \qquad \psi_e = \tfrac{1}{2}(\psi_i + \psi_{i+1}) - \frac{1}{8}(\psi_i + \psi_{i+2} - 2\psi_i)$$

In fact, for the purpose of improving stability the formulae are reorganized as follows

$$\left.\begin{aligned} U_e > 0 \qquad & \psi_e = \frac{1}{8}(5\psi_i + 3\psi_{i+1}) - \frac{1}{8}(\psi_{i-1} - \psi_i) \\ U_e < 0 \qquad & \psi_e = \frac{1}{8}(3\psi_i + 5\psi_{i+1}) - \frac{1}{8}(\psi_{i+2} - \psi_{i+1}) \end{aligned}\right\} \quad (2.5)$$

with the terms in the right-hand parenthesis being treated as 'source' terms, and evaluated using previous-iteration values.

The above treatment is applied in TOROID only for the U and V component. The marching character of the solution in the general flow direction means that an upwind approximation must be retained for the W component. In any event, an upwind approximation is much more satisfactory for the streamwise than the cross-stream components for the flow crossing the upstream and downstream faces does so nearly orthogonally to the control volume face over most of the cross section. Figure 2.3 compares streamwise velocity distributions obtained at 35° from the entry to a circular bend for a simulation covering the first 70° of arc. The entering velocity profile was the parabolic distribution associated with fully developed flow in a straight tube. Two different node densities are employed (the indicated numbers of nodes refer to the θ, ϕ and r directions respectively). There is a moderate difference between the profiles for QUICK and hybrid (i.e. upwind/central) treatments with the finer meshes. Using the coarser mesh, QUICK leads to a distribution of velocity similar to the fine-grid hybrid scheme. Having regard for the earlier calculations of ref [4] there was little doubt that the QUICK results were the more accurate. Even for that scheme, however, one really needs a finer mesh than any used in the above tests to reduce numerical errors to insignificant levels. A modification that allows the desired mesh refinement is summarised in section 2.1.5.

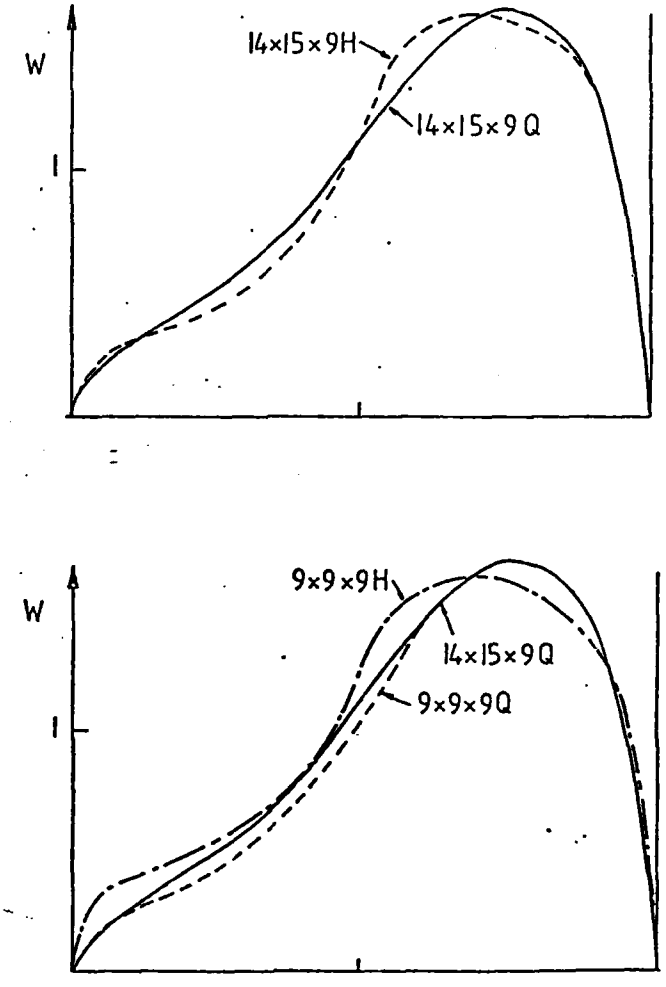

Fig. 2.3 Coarse grid computations comparing HYBRID and QUICK differencing

2.1.4 Boundary Conditions

We consider flow in a round sectioned tube bent in a circular arc. The flow pattern is assumed symmetric about the plane $\phi = 0, \pi$ passing through the centre of the tube. The gradient of V, W, p and T normal to the plane is therefore zero as is likewise the value of U (the velocity normal to the plane). Around the tube surface all velocity components are set to zero.

There has been some controversy in the literature over the handling of boundary conditions at the pipe centre (r = 0). Provided the grid is made fine enough the assumptions made about the boundary values become unimportant (in illustration, one can imagine that a fine but rigid wire bent to follow exactly the locus of the pipe centre would hardly alter the flow pattern from that found with the wire absent). However, the central region is not one where one would wish to concentrate a fine mesh and the coarser the grid the more care needs to be taken.

In the original version of TOROID the radial gradient of all dependent variables was set to zero at the axis. With only nine radial nodes this led to unphysical features in the solution and accordingly the treatment was reformulated. Figure 2.4 shows the locations of nodes in the $r \sim \phi$ plane near r = 0. A central problem is that at the central point many grid nodes are present (each corresponding to a different value of ϕ). For the streamwise velocity component W the same value was assigned to all the central nodes being the average value of W over W(I,2):

$$W(I,1) = \sum_{2}^{NI-1} W(I,2)/(NI-2)$$

The U and V components cannot, however, take the same value at the centre. Instead we required that the resultant of each U and V velocity component must all produce the same velocity vector. Now the resultant velocity must lie along the symmetry axis: its value is taken as the average of the radial velocity components on the symmetry axis either side of the centre node

$$V_{res} = 0.5\ (V(2,3) - V(NI-1,3))$$

The U and V velocity components at the centre are then obtained as

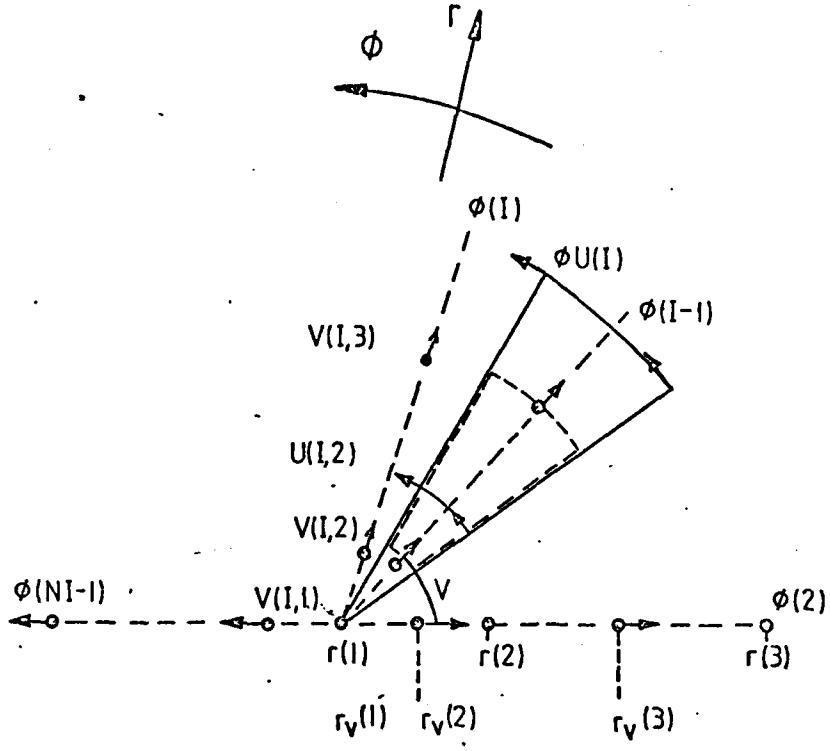

Fig. 2.4 Boundary conditions at tube centre

$$U(I,1) = V_{res} \sin(\phi_U(I))$$

$$V(I,1) = V_{res} \cos(\phi(I))$$

Finally, the ring of nodes V(I,2) is assigned by linearly interpolating between V(I,1) and V(I,3). (This last step is not an essential element of our scheme: one could alternatively obtain V(I,2) by solving the radial momentum equation over the wedge shaped region shown in figure 2.4 as is currently being done by one of Professor Humphrey's students at UC Berkeley).

Figure 2.5 compares profiles of radial velocity across the plane of symmetry for the original and new treatments. Again the computations were those of a 70^{o} bend and the profiles shown are those at 45^{o}. The new version has entirely removed the unphysical discontinuities in velocities that arose with the original.

2.1.5 The Semi-Elliptic Procedure

A semi-elliptic solving procedure is one where in one of the coordinate directions, for all dependent variables except the pressure; information is held to be transmitted only one way, i.e. from "upstream" to "downstream". The practical outcome of this supposition is that these variables do not require storing over the whole solution domain; instead just two planes of storage are provided for each variable (corresponding to the current plane and that immediately upstream thereof) and the computation "marches" from upstream to downstream successively overwriting upstream values held in an array by downstream values on the completion of each new forward step. The pressure must be treated differently from other variables for (in subsonic flow) it is intrinsically affected by the flow in all directions. Indeed, for the flow in a pipe bend, it is the upstream transmission of pressure information from downstream that "warns" the flow that it is approaching the bend and will have to change direction accordingly. The pressure, therefore, must be held over the entire domain and inevitably the solution - not to just the pressure but, by virtue of the coupling of the variables, to the velocity components too - must be obtained by making many sweeps over the domain successively refining the pressure field at each pass.

Thus, a semi-elliptic procedure does not offer a faster route to solution. By drastically reducing the storage requirements, however, it allows, for a given computer installation, a far

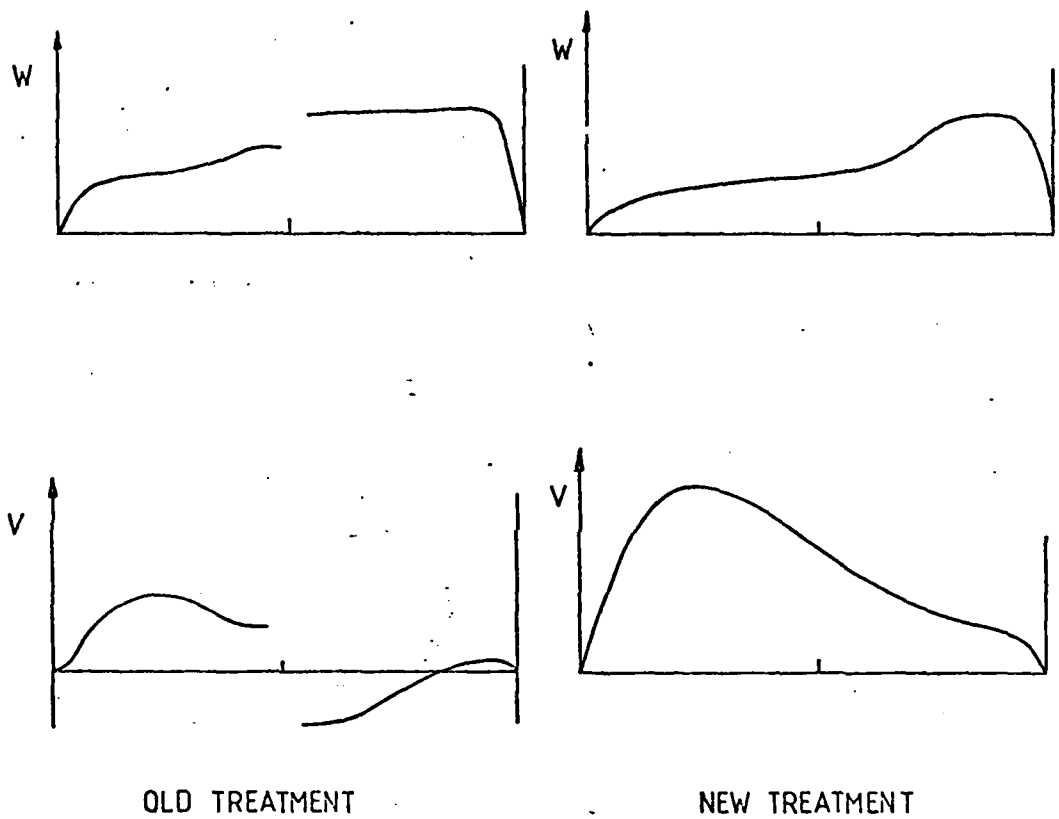

Fig. 2.5 Comparison of axial and radial velocity profiles with new and centre boundary treatments

greater density of grid nodes than with a fully elliptic scheme and thereby brings within the sights of computational feasibility a vast range of complex engineering flows. The 180^{o} tube bend is one flow which, with a CDC 7600 computer, becomes definitely computable with a semi-elliptic scheme. At high Reynolds numbers the only restriction on adopting a semi-elliptic treatment is that there should be no reverse flow regions in the direction of marching. This prevents consideration of flow around very tight bends where separation occurs.

The detailed strategy of a semi-elliptic solving procedure has been set out by Pratap and Spalding [6] and others. A somewhat different sequencing is required than with a fully elliptic solver due to the fact that no velocity field information is available from the previous streamwise sweep over the flow. Figure 2.6 indicates the steps. The diagrams show N, W and P nodes lying on a constant-ϕ surface. (Although the cells are shown as rectilinear a small curvature - about 2^{o} of arc - is present in the θ direction). The nodes are shown by arrows (for velocity) or circles (pressure); solid symbols indicate that the nodal value has been calculated while for open symbols no value is available. The half-filled pressure nodes contain the value of pressure from the previous sweep over the flow domain. At a given step the sequence begins by computing current plane values of V and U (not shown) by solving the respective momentum equations using the pressure from the previous sweep and values for velocity from the upstream station. The streamwise momentum equation is next solved to give the W velocity (displaced a half cell downstream) using "new" values of V and U in the convection terms and presuming a cell mass balance in obtaining the rate of momentum outflow at the downstream face of the control volume.

The final step is the adjustment of the pressure field by the application of the continuity equation to the current-plane pressure cells. Perturbations in the pressure and U and V velocities at the current plane and perturbations in pressure (only) at the upstream plane are introduced to reduce mass-balance errors. Finally, a bulk correction to the downstream pressure is applied to achieve global mass conservation over the tube cross section.

The same sequence of operations is then applied at the next step, and the process successively repeated until the whole domain has been covered. The calculation then begins a further sweep, starting at the upstream plane and proceeding step-by-step over the flow domain using the updated pressure

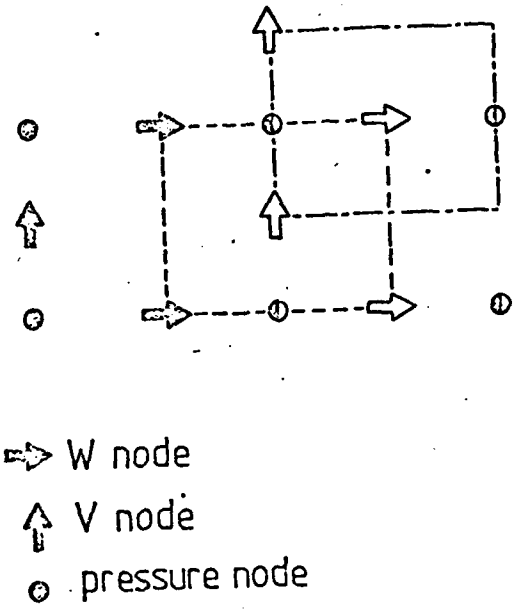

Fig. 2.6 Sequencing of solution with semi-elliptic procedure

field in solving the momentum equations to compute the velocities.

Because the computation as described above has had to make extensive use of "upstream" values instead of current-plane values in evaluating sources and convection coefficients, even when the mass residuals have been reduced to negligibly small levels the pressure and velocity fields will still differ somewhat from those obtained by a fully elliptic solution. It is therefore necessary, as the calculation approaches its (apparent) converged solution to introduce iteration on the velocity components at each step. That is to say, when "current-plane" values have been obtained the velocity equations are re-solved using current values as appropriate in re-forming the coefficients and source terms*. Figure 2.7 shows the very substantial change in the secondary velocity that results from this practice. Due to the non-linearity of the equations three iterations are needed to achieve sensibly asymptotic values (though for industrial calculations or for turbulent flow the additional computing cost would probably not justify going beyond the second iteration).

2.1.6 Application to Flow around a 180° Bend

Agrawal et al [7] have provided a laser Doppler study of laminar flows around a 180° bend over a range of Reynolds numbers and Dean numbers. From these the test at a Dean number of 183 has been selected for computer simulation with the TOROID program. In the computations a uniform streamwise velocity and static pressure have been assumed. The former corresponded closely with the inlet velocity profile reported by the experimenters though inevitably there was a thin boundary layer present whose possible effects cannot be entirely discounted.

---

*Pratap and Spalding [6] apparently omitted this corrective step. That they should have still obtained satisfactory agreement with experiment is presumably because the pipe bend considered in their study was much less severe than that which we are tackling.

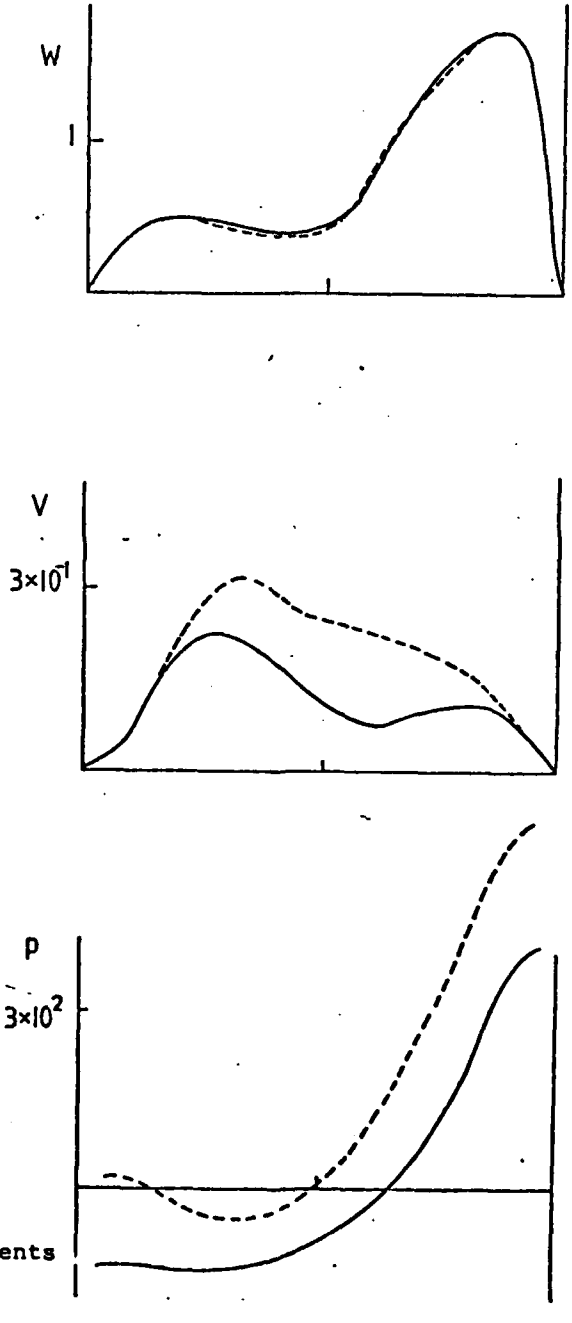

Fig. 2.7 Comparison of semi-elliptic field with elliptic solution

——— elliptic ------- semi-elliptic

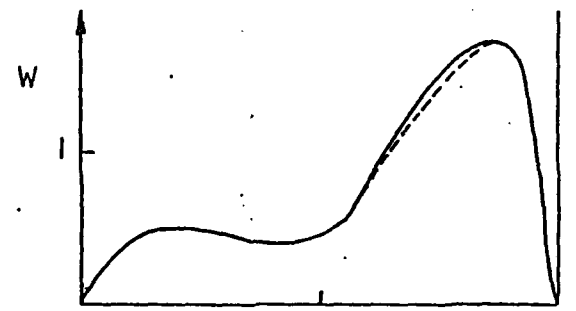

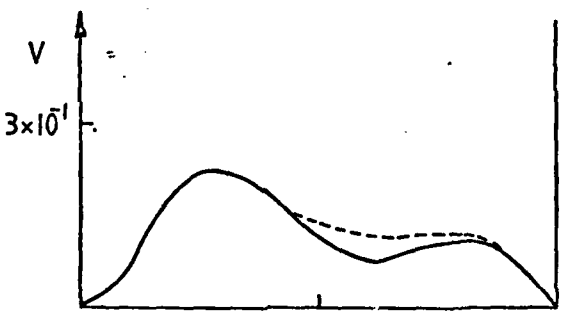

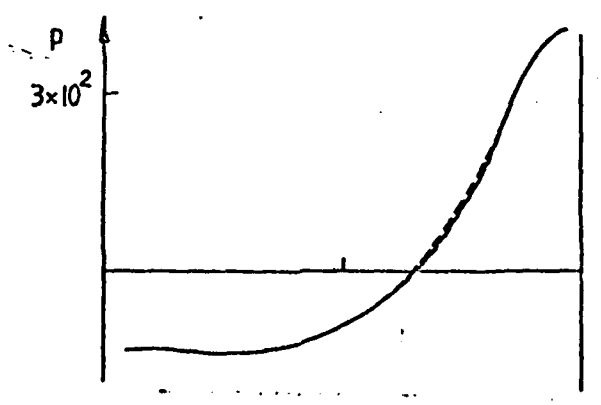

Fig. 2.7

(b) 1 Iteration on velocity field

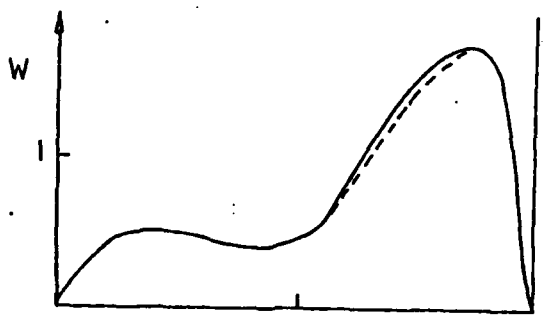

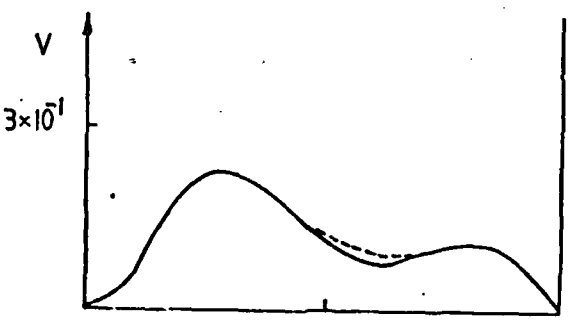

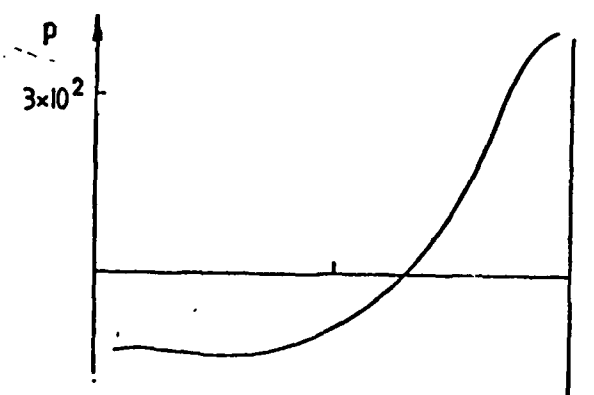

Fig. 2.7

(c) 3 iterations on velocity field

A uniform 20x20 mesh has been used to map the semicircular cross sectional plane with 100 equispaced streamwise sections. Successive sweeps were made until the mass and momentum residual errors summed over all the sections were reduced below 10^{-3} of the entering mass and momentum flows. At exit zero-gradient boundary conditions were applied. This weak constraint, while not particularly accurate, would not be expected to contaminate the solution more than a few tens of degrees inboard from the exit plane. As it happened the last station at which Agrawal report velocity profiles was at 145 degrees, at which position it seems unlikely there would be significant effect on the numerical solution due to uncertainties in the outlet pressure field.

Figure 2.8 compares the measured and computed streamwise velocity profiles along five lines across the pipe cross section and at five streamwise positions. The figures of the measured distributions are taken directly from the published paper; the computer plotted numerical solutions are shown in mirror image and to a slightly different scale. It is nevertheless clear that there is a close degree of correspondence between the measured and computed behaviour. Perhaps the most significant difference between the two is seen at the first station. The computed velocity along the line running closest to the wall is markedly higher than measured while along the other lines agreement is very good. The discrepancy almost certainly arises from neglecting a thin boundary layer at entry to the bend. Since it is the velocity defect of this boundary layer that provides the source term driving the secondary flow around the outer periphery it is consistent that we notice at $\theta = 160^{0}$ (L/R = 19.53) the computed velocity profiles do not exhibit quite as much distortion as the measurements, an indication that the calculated secondary flow is slightly less than in the experiment. Unfortunately, the experimenters do not report secondary velocities at the same Dean number as for the axial flow. Comparisons of the present calculations (for a Dean number of 183) with experiments at a Dean number of 138 at $\theta = 30^{0}$ shown in Figure 2.9 do display broadly similar distributions though, as would be expected, the magnitude of the computed flow is somewhat greater than measured.

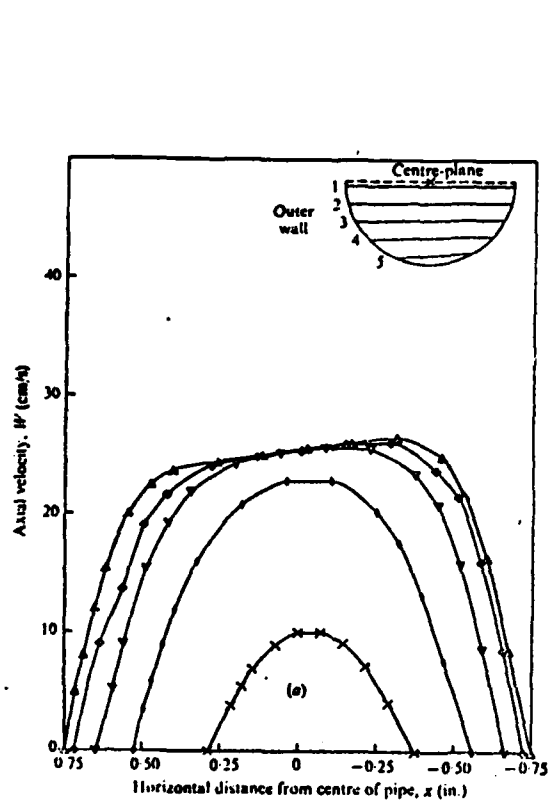

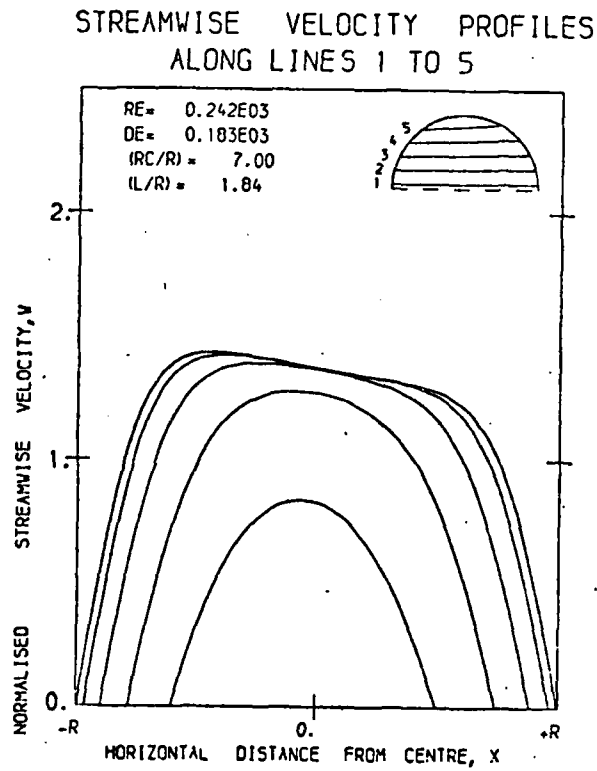

2.8a) L/R = 1.84

Fig. 2.8 Laminar flow around 180° bend with uniform velocity at entry De = 183, Re = 242

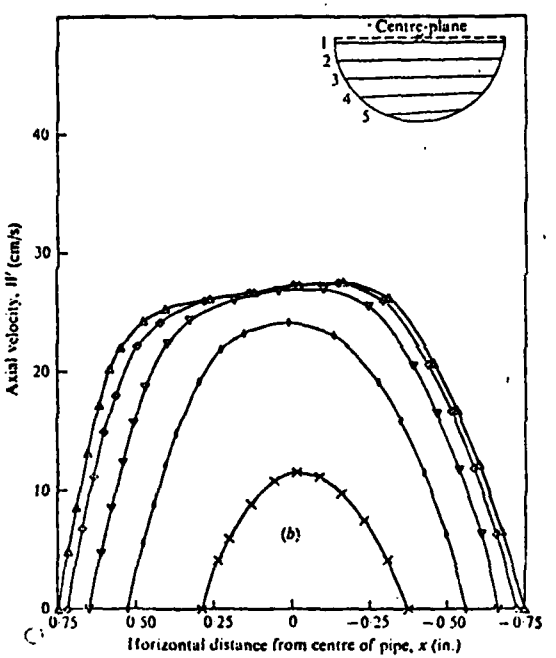

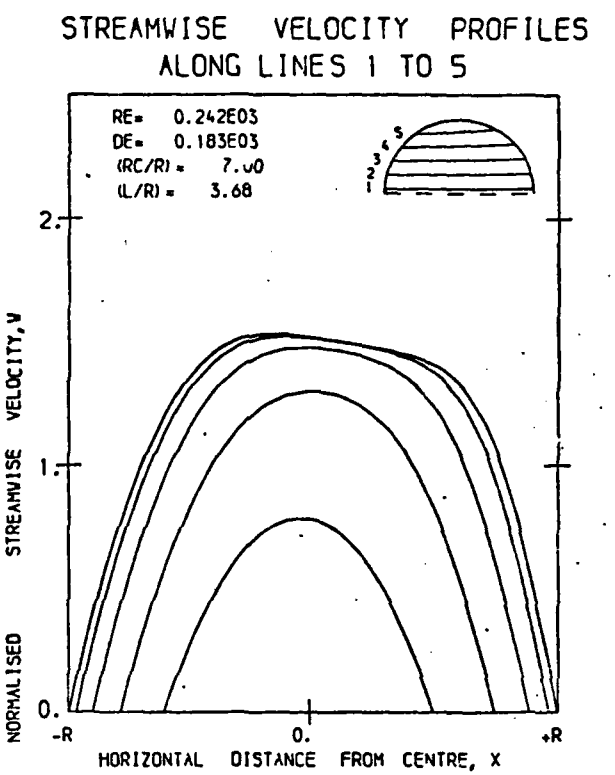

Fig. 2.8b) L/R = 3.68

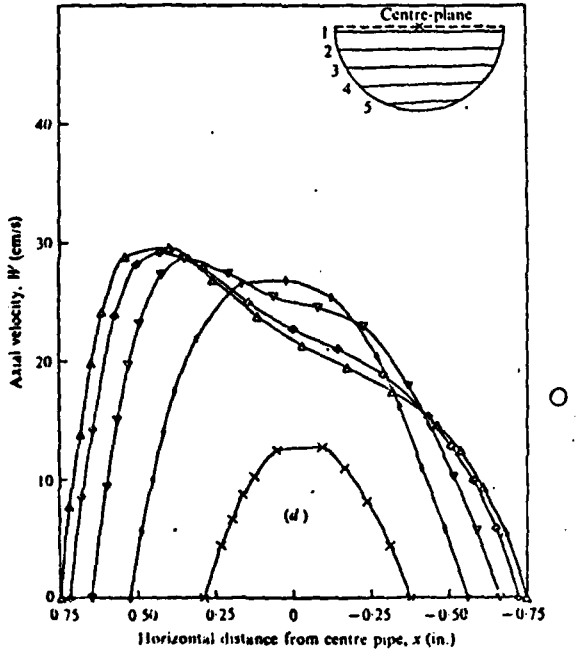

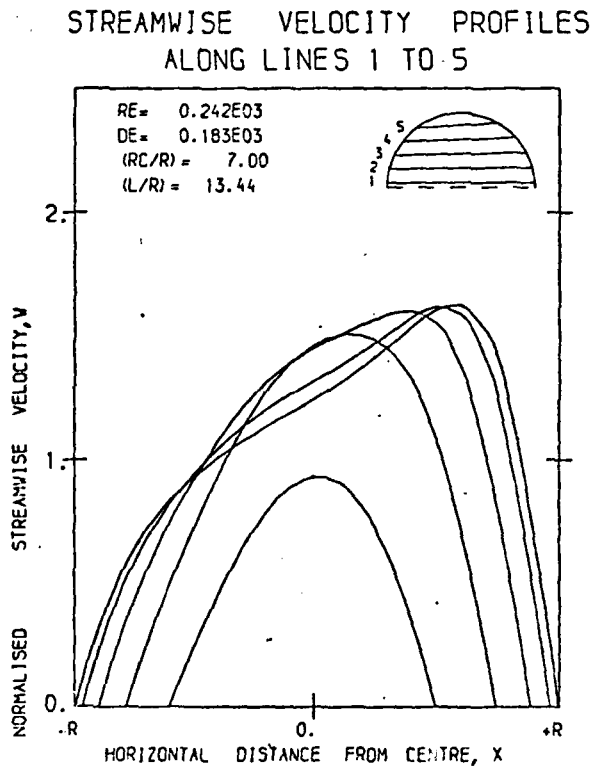

Fig. 2.8c) L/R = 13.44

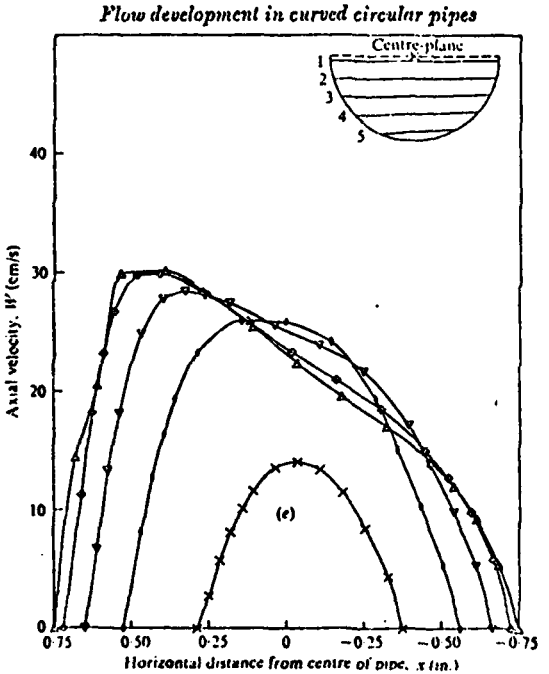
Flow development in curved circular pipes
Centre-plane
1
2
3
4
5
40
30
20
10
0
Axial velocity, W (cm/s)
0·75
0·50
0·25
0
−0·25
−0·50
−0·75
(e)
Horizontal distance from centre of pipe, x (in.)

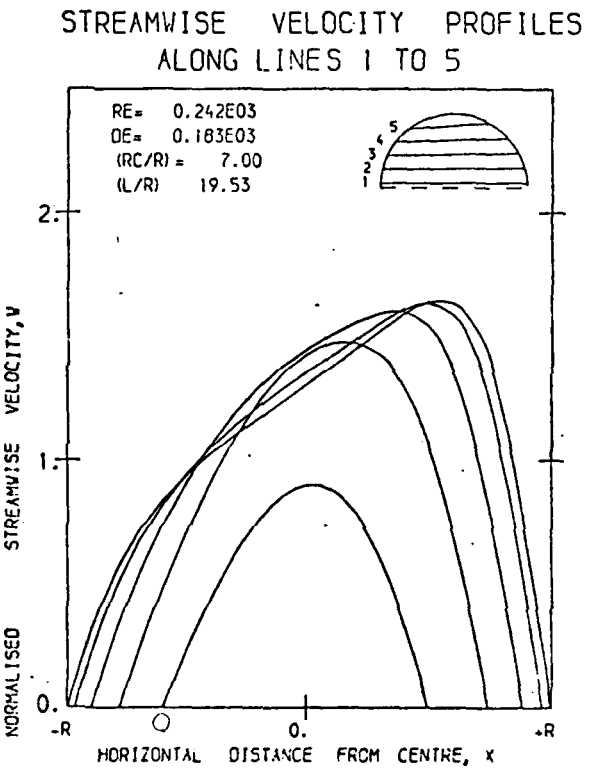
STREAMWISE VELOCITY PROFILES
ALONG LINES 1 TO 5
RE= 0.242E03
DE= 0.183E03
(RC/R) = 7.00
(L/R) 19.53
1
2
3
4
5
2.
1.
0.
NORMALISED STREAMWISE VELOCITY, W
-R
0.
+R
HORIZONTAL DISTANCE FROM CENTRE, X

2.8d) L/R = 19.53

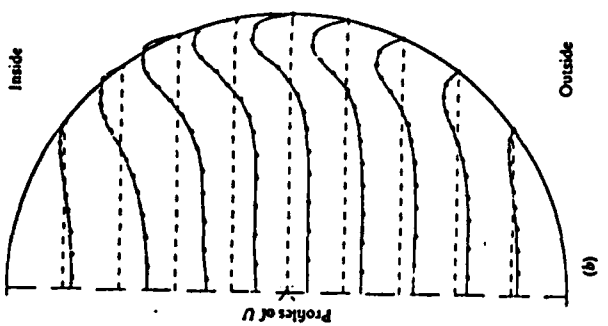

SECONDARY VELOCITY PROFILES

RE= 0.242E03
DE= 0.183E03

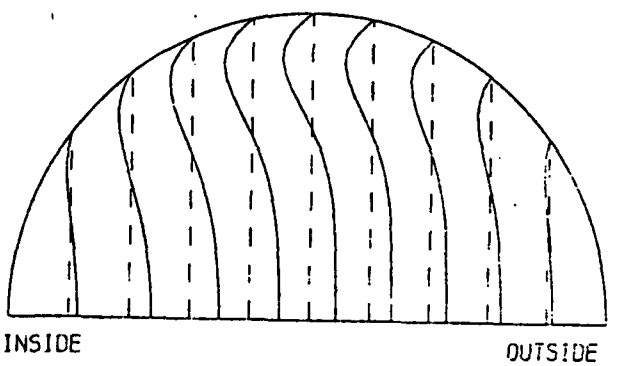

(RC/R) = 7.00
(L/R) = 3.67
DISTANCE BETWEEN ADJACENT DATA LINES
CORRESPONDS TO 36.6% OF BULK VELOCITY

Fig. 2.9 Secondary flow velocities and velocity-direction lines in flow around a 180° bend

2.2 Rectangular Sectioned Duct

2.2.1 Summary of computational work

The program at UMIST has been the beneficiary of the semi-elliptic code developed at Berkeley. The recent report by Humphrey et al. [1] describes this solving procedure and its application to the dynamics of flow around a 180^{o} bend for a duct of square cross-section.

The UMIST effort has consisted of: getting the UCB code mounted on the local computer system (unfortunately this proved a major task due to tape-read problems); incorporating new wall resistance laws; adding the energy equation to allow the thermal field to be calculated; including diagnostics to give a more complete picture of residual errors in solving the 'difference' equations; the introduction of "iterations" on variables other than pressure (as discussed for the toroidal duct in section 2.1); developing plotting codes for printing the results; and, finally, making the computations themselves.

The changes made to the code are discussed in section 2.2.2 while section 2.2.3 presents the computational results and draws comparison with those obtained at Berkeley.

2.2.2 Principal changes to the Berkeley curved duct code

a) multiple iterations

Just as with TOROID, it was found that accurate solution of the momentum equations required iteration of the dependent variables at each plane. This practice allows source terms and convective fluxes which, in the original version, had of necessity to be approximated by corresponding values at the adjacent upstream plane, to be re-evaluated locally. Streamwise variations are so rapid in certain regions of the flow around the bend that a considerably finer mesh than the 3^{o} intervals used in the present work would have been required to make the use of upstream values fully satisfactory.

After explorations with various numbers of local momentum iterations, the practice of 3 iterations per plane was applied as standard. This figure could however have been dropped to 2 without altering the computed values of velocity by more than 1% with a saving of some 22% in computer time.(In this context, '1 iteration' would mean the original practice of using upstream coefficients and proceeding without iteration.)

Given the weaknesses in the present physical model there is no practical benefit in solving the numerical equations to the indicated accuracy. In this research, however, it is desirable to identify the origin of computational error, whether numerical or physical.

b) Aids to Convergence

The multiple iteration practice noted above proved to be highly destabilizing if introduced early in the iteration sequence. Accordingly, only when the pressure field was approaching its 'converged' solution (without iteration) was iteration on the momentum equations introduced; first one iteration, later two etc. In addition formal upstream-downstream under-relaxation, as introduced in Pratap's initial semi-elliptic computations, was used for stability in the initial stages. This practice (as noted earlier with respect to TOROID) had to be switched out before the end of the convergence to avoid errors.

As with TOROID, a diagnosis of the accuracy of convergence of solution of the different equations over the whole domain was added for all dependent variables. With a 'zero' initial field for pressure, 45 sweeps around the bend were needed to reduce the global normalised residual errors below 1% for a 12x22 grid in the cross-stream plane and 103 streamwise planes (of which 60 were in the 180° bend section). The central processor time required for such a calculation for a CDC 7600 computer was 1280 seconds (decimal).

2.2.3 The computed behaviour for the flow in a square sectioned duct around a 180° bend.

The present section discusses computational results for the test geometry studied in the ONR-funded work, a ratio of mean bend radius to hydraulic diameter of 3.35:1. The Reynolds number, 56000, is that used by Professor Humphrey's team in their measurements of the same flow. The present results have all been obtained with the $k-\varepsilon$ Boussinesq viscosity model using standard coefficients. The interest at this level of modelling is: to observe the sensitivity of the results to different wall-boundary treatments, to compare our numerical results with those already obtained by Professor Humphrey's group for the same physical model, and to observe the predicted distribution of heat transfer coefficients. These aspects are considered in turn.

An impression of the effect of the new wall treatment on the veolcity field emerges from figure 2.10a. The 135° position was chosen as this displayed the maximum difference between the two treatments, i.e. the standard (I.C.) treatment and the modified (R.J.) version. For the present flow the most significant difference in the two approaches is that, in the 'RJ' scheme, the wall friction opposing the secondary motion is obtained independently of the streamwise velocity by performing the integration

$$V = \int \{ \frac{\tau_{yx}}{\mu_{eff}} dx \}$$

between the wall and the first node. In contrast, the IC wall treatment assumes that the resultant near-wall velocity parallel to the surface obeys the usual logarithmic law (the streamwise and cross-stream components are then obtained by resolving appropriately). There is very little difference between the velocity fields generated by the two approaches. The effect on the resultant stress and heat flux fields is greater but still relatively small (up to 10%). The result does not indicate that the flow is essentially independent of the nature of the wall law for the secondary motion. When the wall stress opposing the secondary flow is set to zero it is seen from figure 2.10b that quite substantial modifications of the streamwise and axial velocity fields occur. These results indicate that we may have some difficulty in sifting out whether errors due to the physical model arise from the wall treatment or the interior turbulence model. The UMIST heat transfer data will be very helpful in this regard, because, they will be much more sensitive to the wall treatment than is the interior velocity.

Comparisons between the present computations of the velocity field and those obtained by Professor Humphrey's team are shown in figure 2.11 at 45° and 90°. Results obtained from using both QUICK and HYBRID treatments of convection are presented though the former has been established as the more accurate scheme [4 , 8]. There is broadly the same behaviour shown by the independent computations made at the two institutions: our results confirm the prior discovery by our Berkeley colleagues that, with the $k-\varepsilon$ Boussinesq model, both the streamwise and secondary, flow patterns are in substantial disagreement with experiment from 45° onwards.

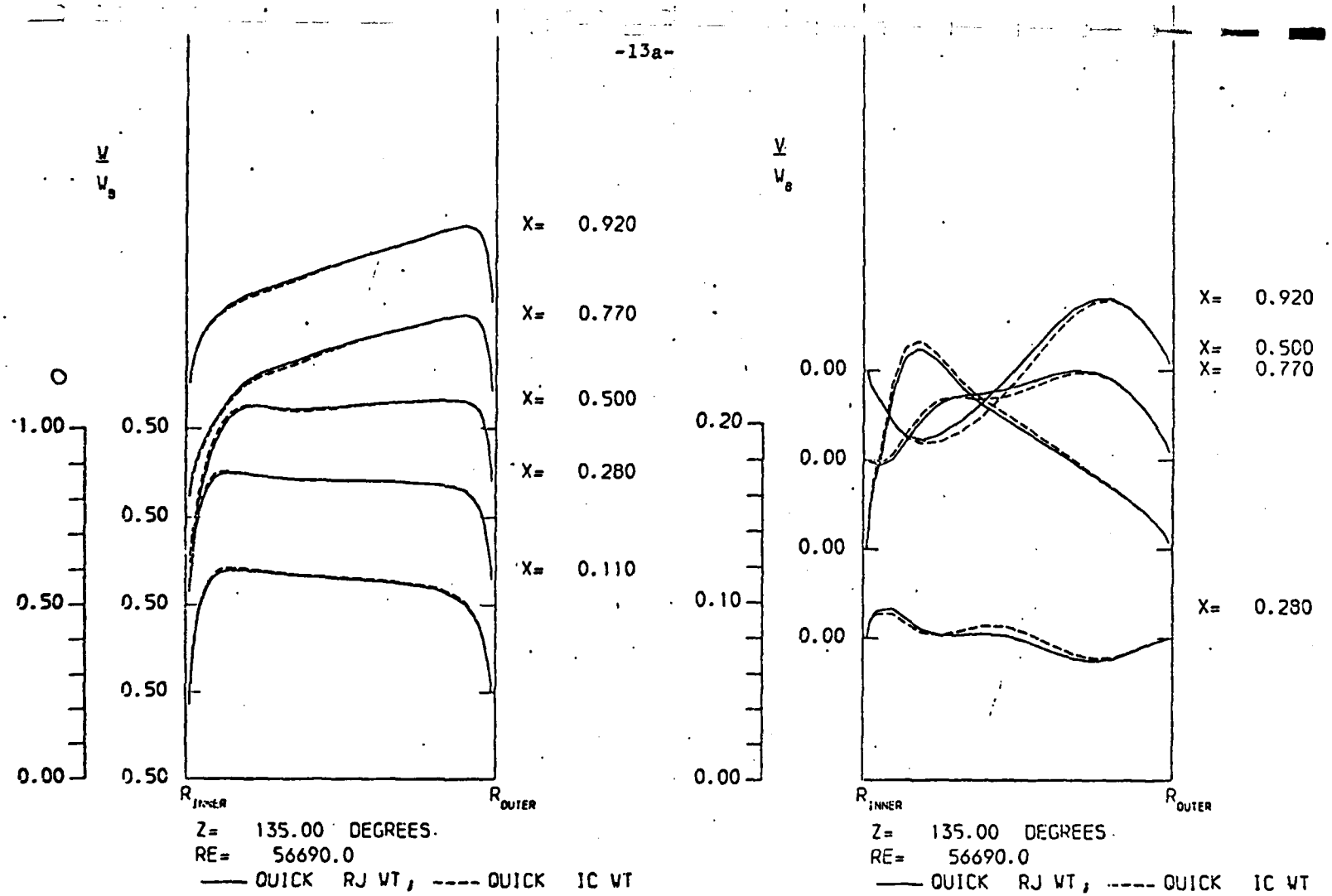

Fig. 2.10 Effects of Near Wall Boundary Treatment

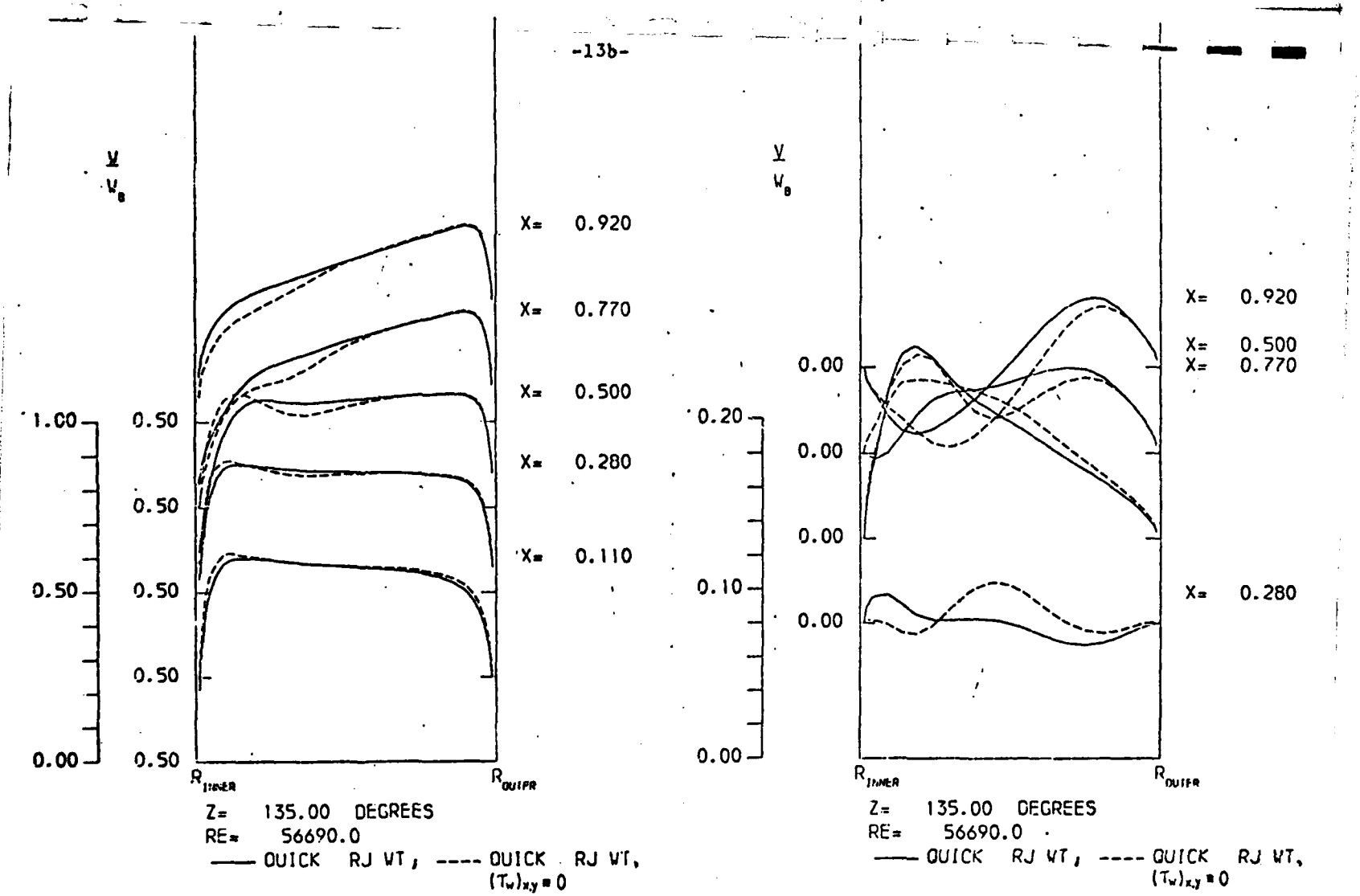

Fig. 2.10 (b) Effects of setting wall shear stress opposing secondary motion to zero

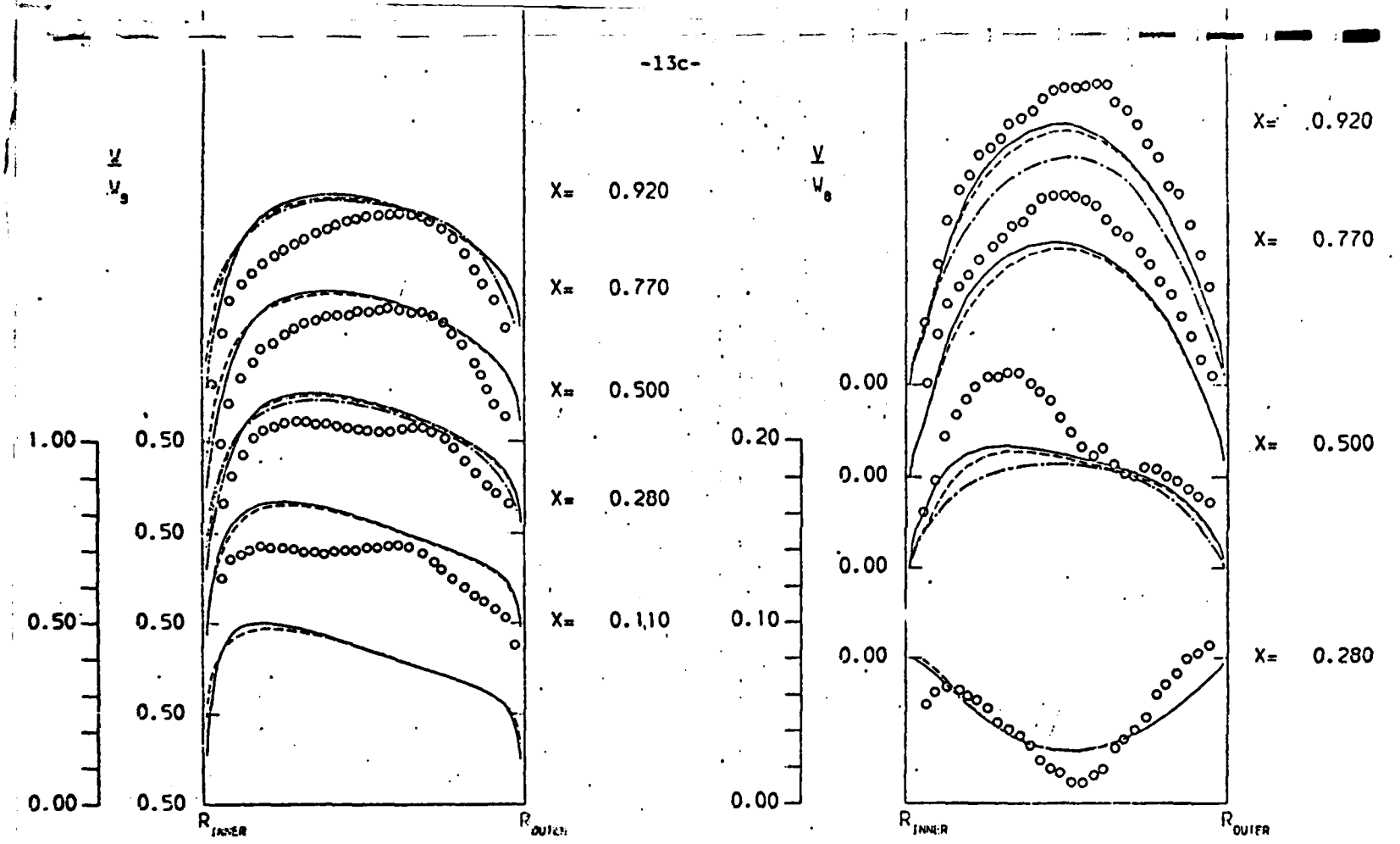

Fig. 2.11 Comparison of present computations with Berkeley computations (a) 45 degrees

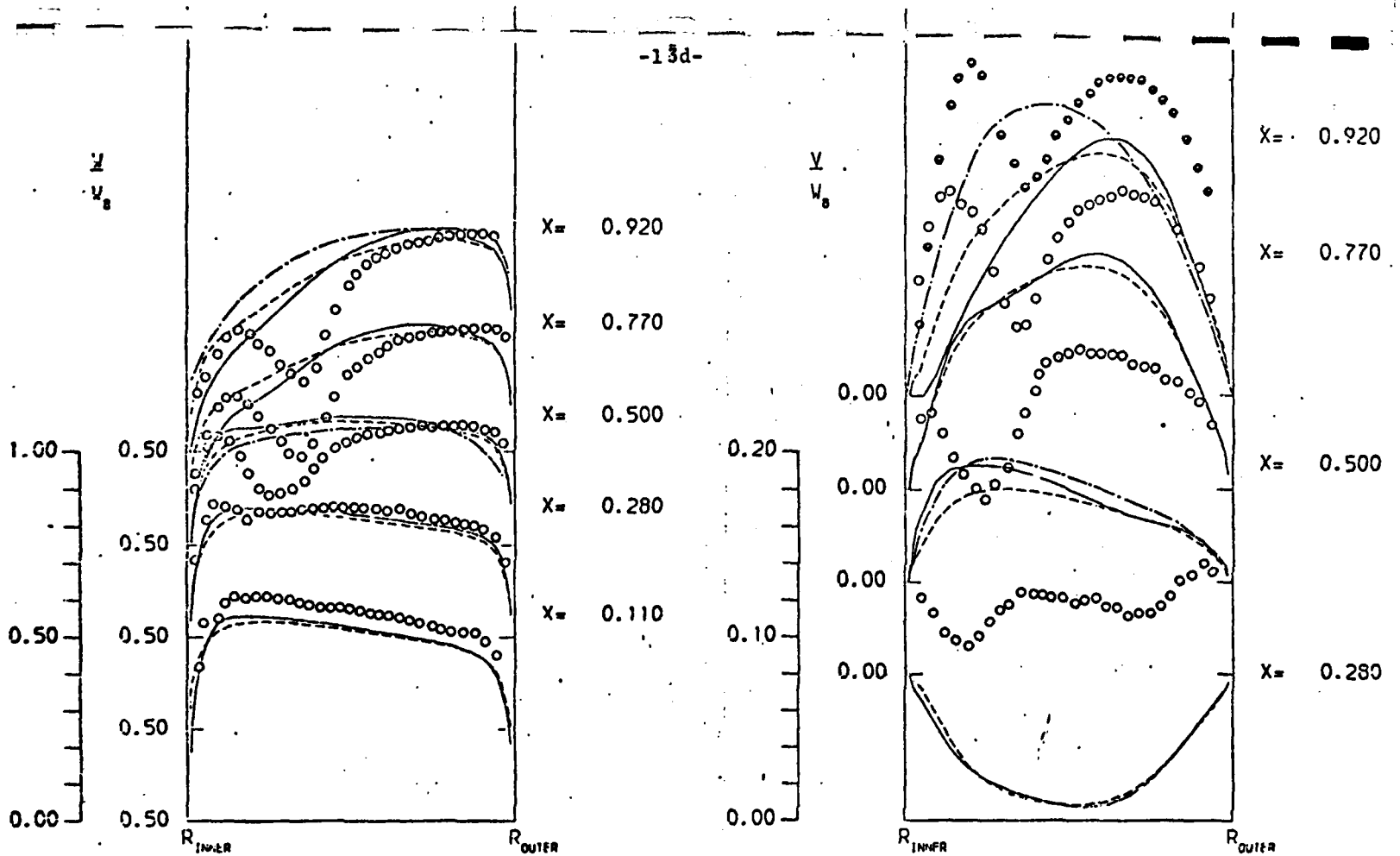

Fig. 2.11 (b) 90 degrees

There are, nevertheless some differences between the computed results obtained at the two institutions that are more serious in the case of the numerically more accurate QUICK scheme(for clarity the Berkeley results with HYBRID are omitted). There are several factors possibly contributing to the differences. To mention but two, the UMIST results used a coarser grid than the Berkeley computations (to allow us to exploit the local computer centre limits on job sizes); on the other hand the present results used current-plane, iterated values of all dependent variables whereas it appears that the Berkeley results may (in common with earlier semi-elliptic treatments) have used upstream values. Clearly the origin of the differences needs identifying and an agreed definitive set of results produced. It is our view that the discovery of variations between our results provides support for there to be planned overlap between research projects a feature that, though incorporated from the beginning in this Berkeley - UMIST collaboration, is rarely built into research programs.

The computed heat transfer pattern in the flow around the bend is shown in figure 2.12. Experimental data are not yet available with which to draw direct comparison though, given the rather poor quality of agreement of the velocity field, it is certain that there will be some significant differences. Nevertheless the broad trends in the observed heat transfer rates are probably not in question. The level of the Nusselt number is strongly affected by the secondary flow. The migration of fluid radially outward near the mid-plane produces slow moving relatively sluggish fluid near the inner wall and associated low-levels of heat transfer coefficient. Correspondingly, fluid impingement on the outer wall causes steep gradients of streamwise velocity and high Nusselt numbers. The ratio of maximum to minimum values of Nu exceeds 2:1 over the second 90^{o} of the bend and downstream therefrom more than 10 hydraulic diameters (the extent of the present computations). It is likely that the actual level of Nusselt number would display rather greater variations than this between the inner and outer surfaces of the bend; for, the exact generation processes associated with mean strain will tend to augment turbulence activity near the concave outer wall while causing damping near the convex inner surface. The algebraic stress model we shall be incorporating in the next phase of our modelling work accounts exactly for these generation processes but the simpler Boussinesq k-ϵ model used here does not.

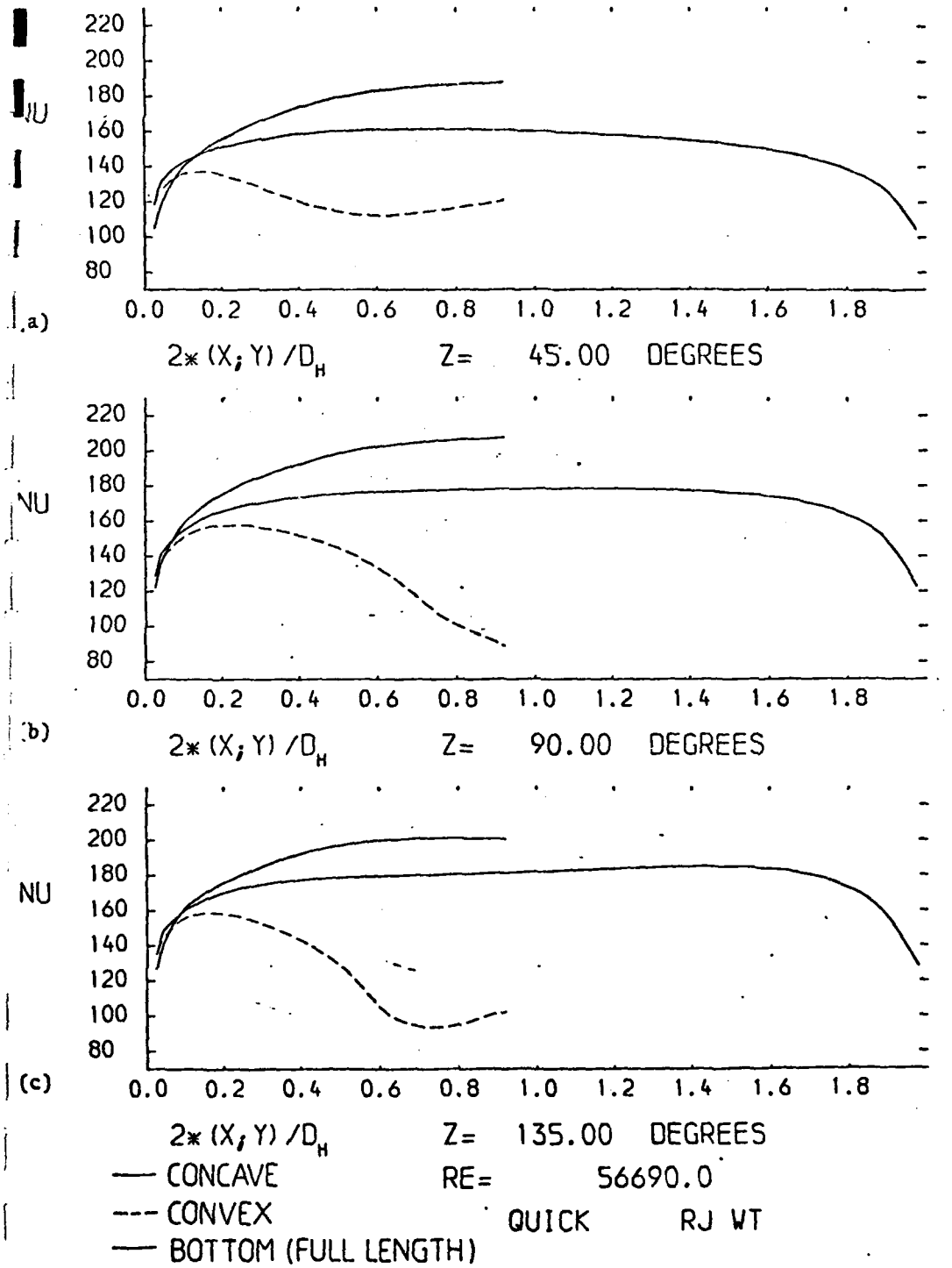

Fig. 2.12 **Computed distribution of Nusselt number in flow around 180° bend (square section duct)**

(a) 45° (b) 90° (c) 135°

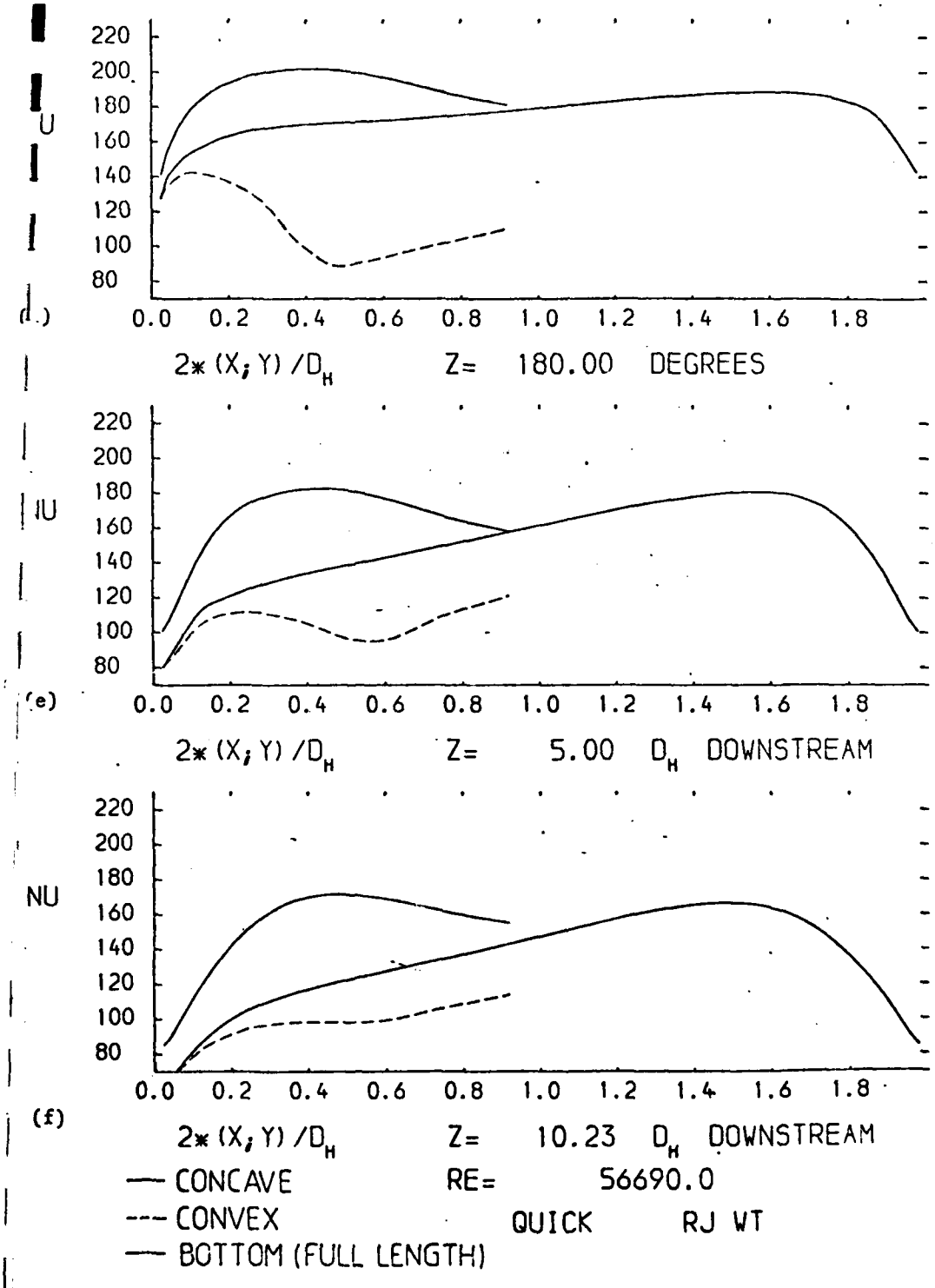

Fig. 2.12 (d) 180° (e) $5.0D_h$ downstream (f) $10D_h$ downstream

We note finally that the Nusselt numbers along the plane sidewalls are fairly uniform in the bend itself and intermediate in magnitude between those on the inner and outer curved walls. The mean Nusselt number given by the Dittus-Boelter correlation is 130 at this Reynolds number whereas the mean computed Nusselt number over the second 90° of bend is in the range 180-195, an augmentation of some 40%.

3. EXPERIMENTAL PROGRAM

The experimental work is running several months behind the schedule foreseen in the last annual report. One of the two major factors contributing to the delay has been the fact that far more machining work to flanges has proved necessary than in the original design. Although the technician time involved has been met by UMIST (rather than the contract budget) there has inevitably been delay because no additional manpower was available. Moreover the emphasis of Richard Johnson's effort has been consciously shifted from experiment to computation, in order that we could obtain predictions of the heat transfer distribution prior to installing the wall thermocouples in the bend. After having obtained the computations of Nusselt number described in the previous section it did indeed appear that some re-arrangement from the original plan was desirable.

The following summarizes the tasks now completed and those still remaining before the definitive tests can be undertaken.

1. The straight and curved sections are completely built including a supporting structure for the apparatus.

2. The fan (in suction mode) has been installed connected and is fully operational.

   Because the electrically heated film would quickly burn out if the fan should fail for any reason a safety cut-out to the heating circuit has been installed.

3. A metering pipe with orifice plates, has been added at the downstream end of the test section to monitor flow rate. This gives a more accurate measurement with better resolution than the originally planned static pressure tappings in the contracting section.

4. Leak tests have been performed showing very good integrity with small leaks easily plugged.

5. Electrical voltage regulating and monitoring equipment has been built and is ready for use to regulate the power applied to the Intrex heating film, including regulation of 14 quarter-inch wide 'tracks' to be inscribed in the intrex used on the flat surfaces around the bend. This special treatment is necessary to ensure a uniform heat flux there (a discussion of this issue is presented in the 1980/81 Annual Report [9]).

6. An inlet contraction section has been constructed and installed in the duct to provide a smooth, uniform inlet velocity profile without separation or other unsteadiness.

7. Fifteen thermocouples at each of 8 axial measuring stations have been installed into the wall of the Plexiglas duct. The thermocouples, will be in contact with the back (untreated) side of the Intrex with silver-loaded epoxy positioned at their measuring junctions to provide accurate temperature measurments.

   Tests have been carried out to measure the temperature drop across the Intrex; this appears to be in the neighbourhood of $0.1^{\circ}C$ or less for the heat fluxes desired.

8. Flow visualization tests have been performed using atomized paraffin droplets and a 'thin slice' laser beam produced by placing a glass tube in front of the beam. The 'thin slice' of light produced was approximately 3 mm thick and wide enough to illuminate the entire cross-section of the duct.

   At present visualization has been successful only at low Reynolds numbers an example of which is shown in figure 3.1. The secondary flow is clearly evident (the assymmetry about the horizontal plane apparent in this figure arose from blockage from the smoke injection since at the time smoke had been introduced only a short distance upstream of the bend).

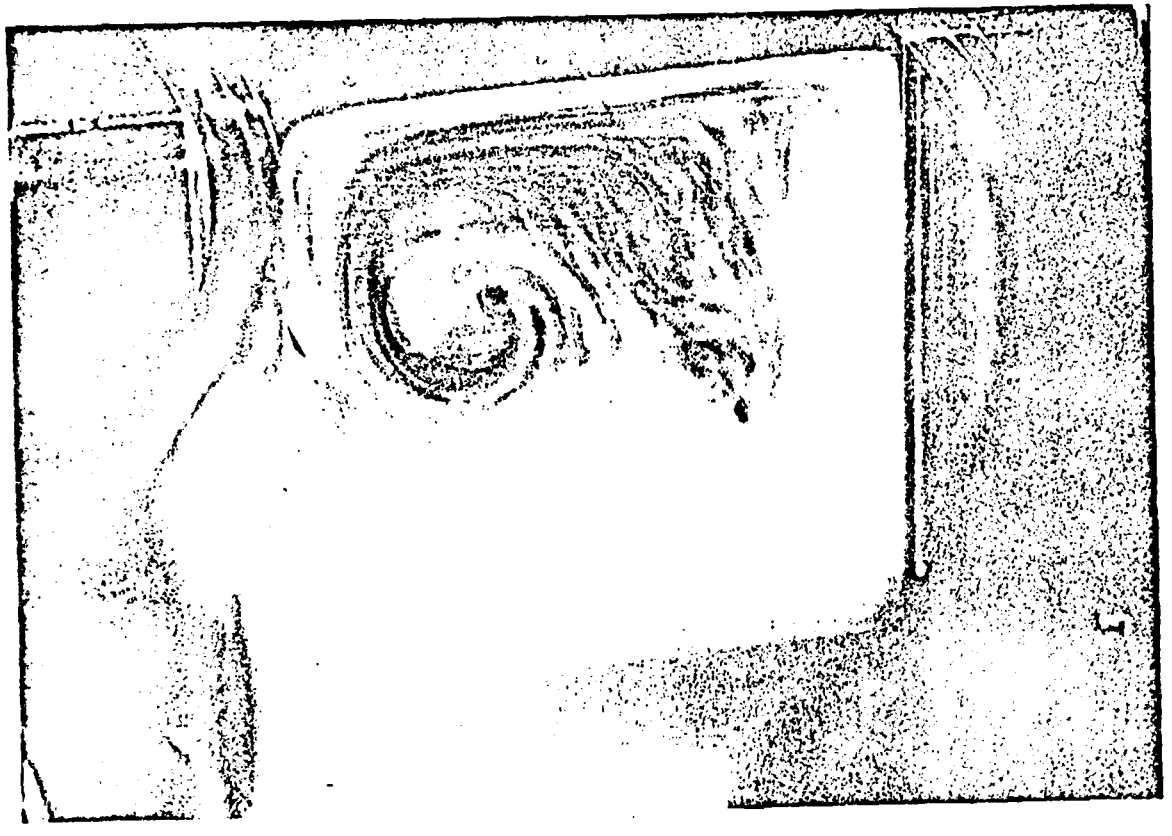

Fig. 3.1 Smoke vizualisation of secondary flow pattern at 90^{o}.

9. The gold-coated Intrex film is about to be installed A good deal of testing of the Intrex has been carried out to establish its resistivity characteristics, the techniques for mounting it on the Plexiglas, the best way of ensuring good electrical contact and the upper voltage limit permitted across the sheet. The various shake down tests have confirmed indications that the Intrex is very suitable for our testing purposes and will be easy to handle and install.

The remaining tasks before the testing programme can begin are:

(a) finish the installation and checking of the Intrex,

(b) final leak testing,

(c) checking of fan, voltage-control systems, manometers,

(d) build temperature rake.

The initial measurements will be a limited mean velocity survey upstream of the bend following which the wall conditions in the first 1m of the inlet duct will be successively adjusted to achieve as closely as possible conditions identical with those of the Berkeley experiments.

ACKNOWLEDGEMENTS

The research has benefitted on many levels from interaction with Professor J.A.C. Humphrey at UC Berkeley and his research student Sheng Ming Chang. To them we express sincere appreciation.

At UMIST Mr. D. Cooper has provided skilful and dedicated assistance in fabricating the test apparatus and Mr. A. Prunty has designed and built various electrical control circuits.

REFERENCES

1. J.A.C. Humphrey, PhD Thesis, Faculty of Engineering, University of London, 1977.

2. S.V. Patankar and D.B. Spalding, Int J. Heat Mass Transfer 15, 1787, 1972.

3. R. Aris, 'Vectors, tensors and the basic equations of fluid mechanics' Prentice Hall, NJ 1962.

4. T.Y. Han, J.A.C. Humphrey and B.E. Launder, Comp. Meth. Appl. Mech. Eng. 29, 81, 1981.

5. B.P. Leonard, Comp. Meth. Appl. Mech. Eng. 19, 59, 1979.

6. S.V. Pratap and D.B. Spalding, Aero. Quart. 26, 219, 1975. (See also S.V. Pratap, PhD Thesis, Faculty of Engineering, University of London, 1975).

7. Agrawal, L. Talbot and K. Gong, J. Fluid Mech. 85, 497, 1978.

8. J.A.C. Humphrey, S.M. Chang and A. Modavi, " Developing turbulent flow in a 180° Bend and downstream tangent of square cross section". 3rd Annual Rep. ONR (Power Program) Contract N00014-8-E0031. University of California, LBL Report 14844, Sept. 1982.

9. B.E. Launder, R.W. Johnson 'Turbulent flow and heat transfer in flow around a 180° bend'. Annual Progress Report for year beginning Nov. 1, 1980, UMIST Mechanial Engineering Department Rep. TFD/82/2.

END

DATE
FILMED

7 83